

# Influence of water and sediment supply on the long-term evolution of alluvial fans and deltas: Statistical characterization of basin-filling sedimentation patterns

Kyle M. Straub<sup>1</sup> and Yinan Wang<sup>1,2</sup>

Received 28 January 2013; revised 13 June 2013; accepted 19 June 2013.

[1] The temporal and spatial variability of sedimentation, resulting from sediment storage and release and the lateral mobility of sediment transporting flows, imparts fundamental patterns into the stratigraphic record. Recent studies show that paleoenvironmental (allogenic) signals preserved in stratigraphy may be contaminated by internally generated (autogenic) sedimentation patterns; however, it is unclear how the magnitude of autogenic dynamics is related to allogenic forcings. Utilizing statistical methods, we quantify basin-filling trends in three laboratory experiments where input water and sediment flux were varied. We use the compensation index and compensation time scale to estimate the strength of compensation, defined here as the tendency to fill topographic lows faster than would result from random deposit stacking, and to estimate the time scales over which autogenic processes operate. In the experiments, topography of channelized deltas formed by noncohesive sediment was monitored in a basin experiencing temporally and spatially uniform relative subsidence. Each experiment resulted in construction of a stratigraphic package in excess of 25 channel depths thick. We find that compensation strength in the experiments is not influenced by absolute magnitudes of water and sediment flux but does increase as a function of the ratio of water to sediment flux. A compensation time scale, defined as the maximum depth of a system's channels divided by the long-term deposition rate, accurately defines the maximum time scale at which autogenic dynamics occur in all experiments. When applied to field-scale systems, we predict that autogenic dynamics occur out to time scales between 5 and 150 kyr.

**Citation:** Straub, K. M., and Y. Wang (2013), Influence of water and sediment supply on the long-term evolution of alluvial fans and deltas: Statistical characterization of basin-filling sedimentation patterns, *J. Geophys. Res. Earth Surf.*, 118, doi:10.1002/jgrf.20095.

## 1. Introduction

[2] The development of basin-scale quantitative stratigraphic models began in 1978 with a study by Pitman that presented the first formal analysis of the relationship between shoreline location and sea level in basins experiencing tectonic subsidence. Following Pitman [1978], development of most quantitative stratigraphic models focused on system boundary conditions and resulting stratigraphic architecture [Allen, 1978; Kendall *et al.*, 1991; Mackey and Bridge, 1995; Karssenberg and Bridge, 2008]. These boundary conditions, or allogenic forcings, include global sea level, tectonic setting, and climate. During the last 10 years,

however, we have witnessed extraordinary growth in the number of studies documenting the importance of internal, or autogenic, dynamics of depositional systems and resulting stratigraphic architecture over a range of time and space scales [Sheets *et al.*, 2002; Kim *et al.*, 2006; Kim and Paola, 2007; Straub *et al.*, 2009; Van Dijk *et al.*, 2009; Hajek *et al.*, 2010; Hofmann *et al.*, 2011]. Importantly, the relatively recent realization that autogenic dynamics occur over time scales important to basin-filling sedimentation patterns suggest further improvements in stratigraphic architecture models will require further quantification of autogenic processes resulting from a range of allogenic forcings.

[3] Modeling stratigraphic architecture has received significant attention as alluvial deposits house important groundwater and hydrocarbon reservoirs and provide reservoirs in which atmospheric carbon dioxide may be sequestered. Further, sedimentary deposits that arise from depositional processes along continental margins serve as home to millions of people. These environments are particularly susceptible to environmental change, resulting from both anthropogenic and natural drivers [Syvitski *et al.*, 2009], making our ability to unlock paleoenvironmental records particularly relevant to our understanding of these systems and our ability to predict

<sup>1</sup>Department of Earth and Environmental Sciences, Tulane University, New Orleans, Louisiana, USA.

<sup>2</sup>Department of Energy Resources Engineering, Stanford University, Stanford, California, USA.

Corresponding author: K. M. Straub, Department of Earth and Environmental Sciences, Tulane University, New Orleans, LA 70118, USA. (kmstraub@tulane.edu)

future system evolution. Development of quantitative stratigraphic interpretation tools could allow us to use the stratigraphic record to query how natural systems responded to a wide spectrum of past environmental forcings and thus aid coastal restoration modeling efforts.

[4] While a range of field, experimental, and numerical studies document autogenic processes and their stratigraphic products, we still have only a cursory understanding of the influence of allogenic forcings (both steady and unsteady in time) on the internal dynamics of sedimentary systems. Studies that do examine how autogenic processes change as a function of allogenic forcings primarily focus on dynamics that occur over micro ( $<10^1$  years) to meso ( $10^1$ – $10^4$  years) time scales (following *Sheets et al.* [2002]). For example, studies by *Bryant et al.* [1995] and *Powell et al.* [2012] have improved our understanding of avulsion dynamics as a function of basin aggradation rate and water and sediment discharge rates. Recent studies that couple experimental and field work, though, suggest that autogenic processes also influence stratigraphic architecture at the macroscale ( $>10^4$  years) [*Straub et al.*, 2009; *Hajek et al.*, 2010; *Wang et al.*, 2011]. While these studies provide convincing evidence for the existence of macroscale stratigraphic products resulting from autogenic processes, no studies have examined how these autogenic products vary as a function of basin boundary conditions. Here we use experiments on fluvial systems experiencing relative subsidence to examine how macroscale autogenic dynamics vary as a function of basin input water flux,  $Q_w$ , and sediment flux,  $Q_s$ .

[5] Results from physical and numerical modeling studies coupled to field data indicate that temporal and spatial variability of sedimentation, here referred to as the evenness of sedimentation, imparts a first-order control on the stratigraphic evolution of sedimentary systems. Under constant or even changing boundary conditions, some sedimentary systems tend to move across and fill basins randomly and chaotically, while others deposit in a structured, even manner. For example, highly mobile fan-delta systems explored in *Sheets et al.* [2007] can migrate across a basin to fill it much more evenly than more cohesive, laterally restricted deltaic systems [*Hoyal and Sheets*, 2009; *Edmonds and Slingerland*, 2010]. Likewise, sedimentary systems that are very large with respect to the size of a basin may be capable of filling space more evenly than smaller systems.

[6] One way of describing how evenly basins fill is to characterize the degree of compensation observed in a sedimentary system. Following *Straub et al.*'s [2009] definition, compensation describes the tendency of flow-event deposits to preferentially fill topographic lows, smoothing out topographic relief and “compensating” for the localization of prior depositional elements. This tendency is thought to result from either a continuous or periodic reorganization of the sediment transport field to minimize potential energy associated with elevation gradients [*Mutti and Sonnino*, 1981; *Stow and Johansson*, 2000; *Deptuck et al.*, 2008]. This tendency can be seen in avulsions, which often occur following the aggradation of a channel bottom to an elevation equivalent or greater than the bordering floodplain, at which time channels become prone to avulse during flood events [*Mohrig et al.*, 2000]. Compensational stacking has been used to describe the large-scale architecture of deepwater and fluvial deposits, and, in particular, delta packages

[*Olariu and Bhattacharya*, 2006; *Hofmann et al.*, 2011; *Hajek et al.*, 2012], wherein periodic channel or lobe avulsions occur, reorganizing the sediment transport field along local topographic lows.

[7] *Straub et al.* [2009] followed shortly thereafter by *Wang et al.* [2011] were the first to quantitatively examine the strength of compensation in alluvial basins. The compensation index,  $\kappa$ , as proposed by *Straub et al.* [2009] uses the rate of decay of spatial variability in sedimentation between picked depositional horizons with increasing stratigraphic averaging distance. This metric allows quantification of observed stacking patterns in subsiding basins to what would be expected from uncorrelated random stacking. Using physical experiments, numerical models, and field data, *Wang et al.* [2011] used changes in the compensation index as a function of measurement interval to show that compensation is scale-dependent and can be used to estimate autogenic time scales in channelized sedimentary deposits.

[8] Following *Straub et al.* [2009] and *Wang et al.* [2011], we use data from three physical fluvial-deltaic experiments experiencing relative subsidence in an experimental basin to characterize basin-filling sedimentation patterns. Here we focus on the influence of  $Q_w$  and  $Q_s$  and their ratio,  $Q_w:Q_s$ , on the strength of compensation and the time scales over which autogenic processes operate. We choose to examine the influence of  $Q_w$  and  $Q_s$  in addition to their relative ratio as several recent studies note that these parameters influence autogenic time scales and the lateral mobility of transport systems [*Clarke et al.*, 2010; *Kim et al.*, 2010; *Powell et al.*, 2012]. Each experiment described below has its own constant boundary conditions, with  $Q_w$  and  $Q_s$  varying between experiments. We choose to explore systems with temporally constant boundary conditions as a first step toward defining the relationship between allogenic forcings and autogenic processes. Future work will likely be needed to understand how autogenic processes respond to temporally unsteady boundary conditions. Results from these experiments are then used to explore possible time scales over which autogenic processes operate for fans and deltas at field scale.

## 2. Compensation Index and Time Scale

[9] In this section we present theory developed by *Straub et al.* [2009] and *Wang et al.* [2011] that we use to quantify the strength of compensation in alluvial basins and the time scales over which autogenic processes operate. For convenience, we re-present this theory below.

[10] *Straub et al.* [2009] quantified compensation in basin filling by comparing the spatial variability in sedimentation between selected depositional horizons with increasing vertical stratigraphic averaging interval. We define the standard deviation of sedimentation/subsidence ( $\sigma_{ss}$ ) as

$$\sigma_{ss}(T) = \left( \int_L \left[ \frac{r(T;x)}{\bar{r}(x)} - 1 \right]^2 dL \right)^{1/2} \quad (1)$$

where  $r(T;x)$  is the local sedimentation rate measured over a stratigraphic interval of duration  $T$ ,  $x$  is a horizontal coordinate,  $L$  is the cross-basin length, and  $\bar{r}(x)$  is the local long-term sedimentation (or subsidence) rate. The value of  $\sigma_{ss}$  serves as a measure of the extent of subsidence control on the magnitude and spatial pattern of deposition in a basin.

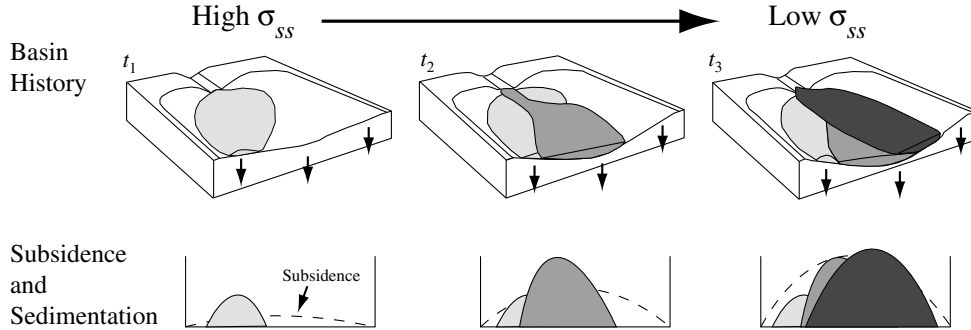


**Figure 1.** Schematic following Lyons [2004] describing the progression of a basin toward equilibrium. In the block diagrams illustrating basin history, subsidence (indicated by arrows) is temporally constant but spatially variable. Sedimentation represented by lobes of different color is temporally and spatially variable. The balance between sedimentation and subsidence for an arbitrary cross section at the three time steps is represented graphically below each block. At the earliest time,  $t_1$ , subsidence is small and sedimentation is local resulting in a poor fit between the two. However, as the basin develops, subsidence increases, and the sedimentary system has an opportunity to occupy a larger fraction of the total area. The result then, at later times  $t_2$  and  $t_3$ , is that the fit between sedimentation and subsidence improves. Taking the ratio of sedimentation over subsidence pointwise across the basin for each time step would produce ratio distributions with decreasing standard deviations over time.

For example, over sufficiently long time intervals, a sediment transport system has time to visit every spot in a basin repeatedly, and as a result, the ratio of the local sedimentation rate to subsidence at all locations in the basin is close to unity (Figure 1). Over short time intervals, however, depositional geometries within a basin are controlled by the configuration of the transport system. As a result, the ratio of sedimentation to subsidence at any one point in the basin is highly variable. Straub *et al.* showed that  $\sigma_{ss}$  decreases with increasing  $T$ , following a power-law trend for six study basins

$$\sigma_{ss} = \gamma T^{-\kappa} \quad (2)$$

where the exponent,  $\kappa$ , was termed the compensation index and  $\gamma$  is a leading coefficient whose units change depending on the value of  $\kappa$  and defines the magnitude of  $\sigma_{ss}$  at  $T$  equals 1. Specifically, the units of  $\gamma$  equal  $T^\kappa$ .  $\kappa$  was found theoretically to be 0.5 for random stacking that is uncorrelated in space and time, and 1.0 for perfect compensational stacking. Values less than 0.5 indicate anticompensation or persistence in depositional trends.

[11] In the above framework, one can distinguish stratigraphy characterized by random processes from stratigraphy resulting from nonrandom processes. Here we define stratigraphic organization as the degree to which depositional elements stack in a nonrandom fashion. With this definition, we note that there are two ways to move away from randomness. The first involves increasing  $\kappa$  from 0.5 to 1, which results in depositional trends which progress toward compensation faster than would be expected from random stacking. The second involves decreasing  $\kappa$  from 0.5 to 0, which results in greater depositional persistence than expected from random stacking. We note that the two methods to move away from randomness in the surface statistics are analogous to the two methods to move away from randomness in point statistics when discussing the distribution of channel bodies in stratigraphy [Hajek *et al.*, 2010]. For the remainder of this manuscript, we refer to the strength of organization as the magnitude to which  $\kappa$  varies from 0.5.

[12] Wang *et al.* [2011] examined how  $\kappa$  varies as a function of measurement window and found it to be scale-dependent. Specifically, using data from physical experiments, numerical models, and field-scale outcrops, they observed a scale break in the decay of  $\sigma_{ss}$  as a function of  $T$ . Wang *et al.* defined the compensation time scale,  $T_c$ , as the time at which this scale break occurs. Further,  $T_c$  was found to occur at a time scale set by the maximum scale of surface roughness,  $l$ , in a transport system divided by the long-term aggradation rate

$$T_c = \frac{l}{\bar{r}} \quad (3)$$

[13] For experimental systems, it was found that the maximum depth of a system's channels,  $H_c$ , well approximated  $l$ . The use of  $H_c$  as an important vertical length scale in delta dynamics has also been reported in other studies [Straub *et al.*, 2009; Ganti *et al.*, 2011]. For clarification, we stress here that  $T_c$  does not equal the time scale of avulsion,  $T_A$ , as initially defined by Mohrig *et al.* [2000].  $T_A$  is defined as the depth of a system's channels divided by the in-channel, local aggradation rate, during one avulsion cycle. The scale break identified by Wang *et al.* separates shorter time scales over which  $\sigma_{ss}$  decays with  $\kappa$  less than 1 from longer time scales where  $\kappa$  equals 1. This result suggests that after  $T_c$ , the stacking of deposits is purely controlled by allogenic forcings, while before  $T_c$ , the stacking of deposits is at least somewhat influenced by stochastic autogenic processes (Figure 2).  $T_c$  can also be thought of as the time necessary to transfer a geomorphic surface to a subsurface depth great enough that it is no longer susceptible to reworking by channel migration and thus frozen in the stratigraphic record [Straub and Esposito, 2013]. This formulation is similar to a time scale proposed by Sadler [1993] for deposits to reach a depth such that they are no longer susceptible to reworking by sediment mixing processes and storms. Below, we use results from physical experiments to examine how input basin  $Q_w$  and  $Q_s$  influence the magnitude of  $\kappa$  below  $T_c$ , and

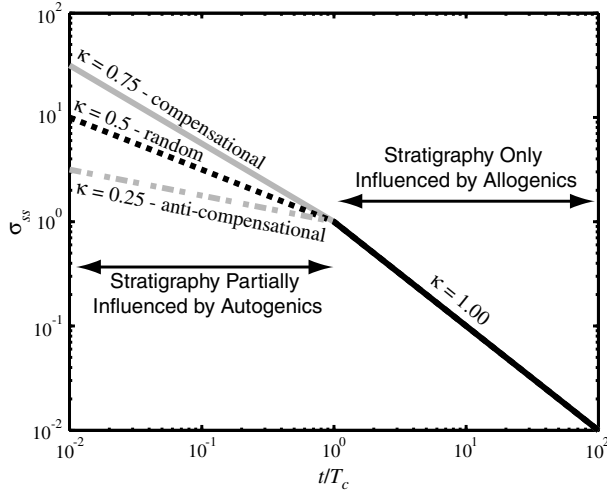


**Figure 2.** Decay of  $\sigma_{ss}$  as a function of  $t/T_c$  for three hypothetical basins. For all basins, the decay of  $\sigma_{ss}$  with time is characterized by a  $\kappa$  equal to 1 at time scales greater than  $t/T_c$  of 1. Over these time scales, basin filling is only influenced by allogenic forcings. Below  $t/T_c$  equal to 1, however, the three basins are characterized by stochastic autogenics of varying magnitude and thus varying  $\kappa$ . For all systems, though, basin-filling trends and resulting stratigraphy are partially influenced by autogenic processes for time scales less than  $t/T_c = 1$ .

thus the strength of autogenic processes, in addition to examining the surface processes and resulting stratigraphy associated with these processes.

### 3. Experimental Methods

[14] To examine the influence of  $Q_w$  and  $Q_s$  and their relative ratio on the strength of autogenic processes over a range of time and space scales, we performed three physical laboratory experiments. A recent review paper on experimental sedimentology and stratigraphy by Paola *et al.* [2009] detailed the wide variety of environments and processes that have been explored at reduced scale, including delta processes and their resulting stratigraphy. While directly upscaling experimental systems to field scale remains challenging, the existence of scale independence in some aspects

of sediment transport and morphodynamics allow experimental systems to produce spatial structure and kinematics that, although imperfect, compare well with natural systems. As a result, these experiments provide morphodynamic and stratigraphic insight into the evolution of channelized settings under an array of external and internal influences.

[15] The three experiments performed in this study were conducted in the Delta Basin at Tulane University's Sediment Dynamics Laboratory (Figure 3). This basin is 2.8 m wide by 4.2 m long and 0.65 m deep. Accommodation is created in the Delta Basin by slowly increasing base level using a motorized weir that is in hydraulic communication with the basin. This system allows base-level control through a computer interface with sub-millimeter-scale resolution. Water and sediment supply to the basin are also controlled through the above mentioned computer interface.

[16] All experiments began with an initial stage with no relative subsidence. During this stage, sediment and water were mixed in a funnel and fed from a single point source at the center of the upstream wall. After a system prograded 3.1 m from the source to shoreline, the main stage of each experiment started. During this stage, base level increased at a rate equal to the total sediment discharge divided by the desired delta-top area. In each experiment, the combination of sediment feed rate and base-level rise allowed the shoreline to be maintained at an approximately constant location through the course of the experiment.

[17] The three experiments had unique combinations of input  $Q_w$  and  $Q_s$  and base-level rise rate (Table 1). The first experiment, TDB-10-1, acted as the control experiment for the study and had input  $Q_w$  and  $Q_s$  and base-level rise rate ( $\bar{r}$ ) of 0.451 L/s, 0.011 L/s, and 5 mm/h, respectively. As such,  $Q_w:Q_s$  in this experiment was 41:1. In the second experiment, TDB-10-2, we doubled  $Q_w$ ,  $Q_s$ , and  $\bar{r}$  relative to TDB-10-1. As both  $Q_w$  and  $Q_s$  doubled relative to TDB-10-1, the two experiments share the same relative ratio of  $Q_w:Q_s$ . Finally, in the third experiment, TDB-11-1,  $Q_w$  doubled relative to TDB-10-1, but  $Q_s$  and  $\bar{r}$  were set equal to the control experiment, resulting in a  $Q_w:Q_s$  twice TDB-10-1.

[18] The sediment mixture used in all experiments was composed of 70% by volume quartz sand ( $D_{50} = 110 \mu\text{m}$ ) and 30% coal sand ( $D_{50} = 440 \mu\text{m}$ ). The coal has a specific gravity of 1.3, whereas quartz has a specific gravity of 2.65, so the coal grains are substantially more mobile than the

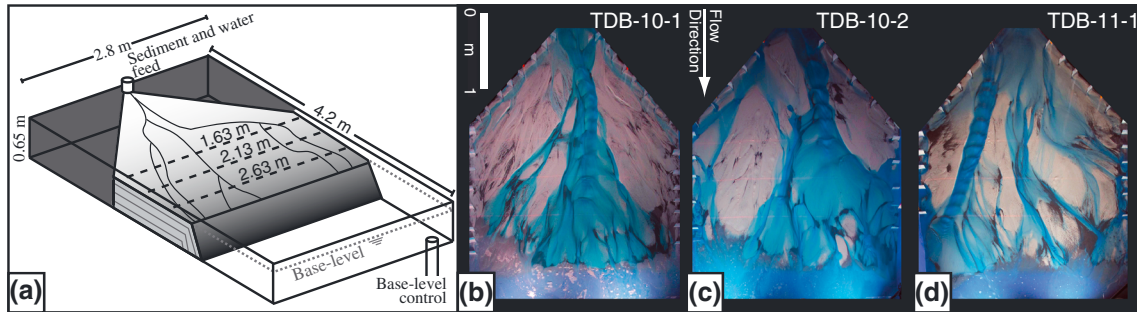


**Figure 3.** (a) Schematic diagram of Tulane Delta Basin facility. Positions of topographic transects are indicated by black dashed lines on fluvial surface. Note that base-level control is in the opposite corner from infeed point. Photographs of active delta tops during (b) TDB-10-1, (c) TDB-10-2, and (d) TDB-11-1, respectively.

**Table 1.** Experimental Boundary Conditions

	Duration	$Q_w$	$Q_s$	$Q_w/Q_s$	Base-Level Rise Rate
	(h)	(L/s)	(L/s)	(1/1)	(mm/h)
TDB-10-1	78.2	0.451	0.011	41	5
TDB-10-2	39.3	0.902	0.022	41	10
TDB-11-1	77.2	0.902	0.011	82	5

quartz grains and serve as a proxy for fine-grained clastics. The mixture of quartz and coal is similar to that used in previous experiments [Heller *et al.*, 2001; Sheets *et al.*, 2007; Martin *et al.*, 2009]. In order to visualize the active channel network, the input water was dyed with a commercially available blue food coloring and made opaque by adding a small amount of titanium dioxide.

[19] Three types of data were collected from the experiments: system morphology, surface topography, and deposit stratigraphy. The morphologies of the fluvial systems were recorded with two digital cameras. One of the cameras was positioned to collect images of the entire basin, which were used to characterize surface dynamics, while the second camera was positioned to collect both surface morphology and topography data. Images of surface morphology were postprocessed to remove camera distortion, resulting in images with horizontal resolution of approximately 0.7 pixels per mm. Both cameras recorded images of the active delta top at 1 min intervals. Topographic measurements were taken in a manner modeled on the XES subaerial laser topography scanner [Sheets *et al.*, 2007]. In contrast to XES, however, where the topography of the entire fluvial surface is recorded periodically, we chose to monitor topography at 2 min intervals along three flow-perpendicular transects, located 1.6 m, 2.1 m, and 2.6 m from the infeed point. This system uses oblique digital images of lines cast by vertical laser sheets from which true topography can be calculated. To measure a full cross section of topography, including areas inundated by water, the experiment was stopped every 2 min, and water was allowed to drain off the fluvial surface prior to collecting measurements. This arrangement allows instantaneous (the exposure time of the camera) measurements. With this system, we obtained measurements with horizontal and vertical resolution of  $\sim 1.0$  mm. The three experiments each produced an average of 415 mm of stratigraphy. Following each experiment, we sectioned and imaged the deposits at each of the topographic strike transects.

#### 4. Experimental Results

[20] In this section, we summarize the statistics that characterize the surface morphology and dynamics of the three experiments. Our aim is to characterize the full range of time and space scales important for basin-filling sedimentation patterns in our three experiments. Aggradation of each fan-delta resulted from the transport and deposition of sediment by migrating channelized flow (Figure 3). Long-term aggradation in each experiment was promoted by steady base-level rise which when coupled to the steady input  $Q_w$  and  $Q_s$  resulted in systems with little net shoreline movement during the main stage of each experiment. Space-time-elevation maps at each measurement transect in the three experiments show a steady long-term deposition rate. In Figure 4, we present an example space-time-elevation map from the

proximal transect of TDB-10-1. While the steady long-term elevation drift is the primary signal visible, careful inspection reveals that the evolution of topography was neither steady in space nor in time over short time scales.

[21] Theoretical, experimental, and field works indicate that  $Q_w$ ,  $Q_s$ , and their relative ratio influence the hydraulic geometry and slopes of channels on alluvial fans and deltas in addition to their morphodynamics [Parker *et al.*, 1998a; Parker *et al.*, 1998b; Whipple *et al.*, 1998; Powell *et al.*, 2012]. As such, prior to characterizing basin-filling trends, we characterize these morphological parameters in our experiments. Utilizing coregistered topographic scans and images of the active transport system, we generate distributions of flow depth for each experiment at each transect. As we are primarily interested in maximum flow depth, we estimate  $H_c$  by the value corresponding to the 95th percentile on cumulative distribution plots of flow depth (Table 2). We find a decrease in  $H_c$  with distance down the dominant transport direction in each experiment and note that  $H_c$  at any one transect location is similar for TDB-10-2 and TDB-11-1, which are greater than that of TDB-10-1.

[22] Next, we estimate the average wetted fraction,  $B_f$ , at the three measurement transects for the three experiments.  $B_f$  is equal to the total wetted width of the transport system divided by the total basin width. We use  $B_f$  as a proxy for channel width as the high width-to-depth ratio of much of the experimental flows makes directly measuring channel width difficult. We measure  $B_f$  using our data set of overhead images of the active transport system. Using a threshold blue luminosity value, we separate wet regions from dry regions on the delta top, given that the input water was dyed blue. The threshold value used for this operation was picked by identifying a value that on visual inspection appeared to correctly separate the two regions. Using the binary images, we calculate the fraction of cross-basin length inundated with water for each image, which allows us to calculate  $B_f$ . We find that on average,  $B_f$  increases down transport system and that at any one transect location, TDB-10-2 has the greatest wetted width followed by TDB-11-1 and then TDB-10-1 (Table 2).

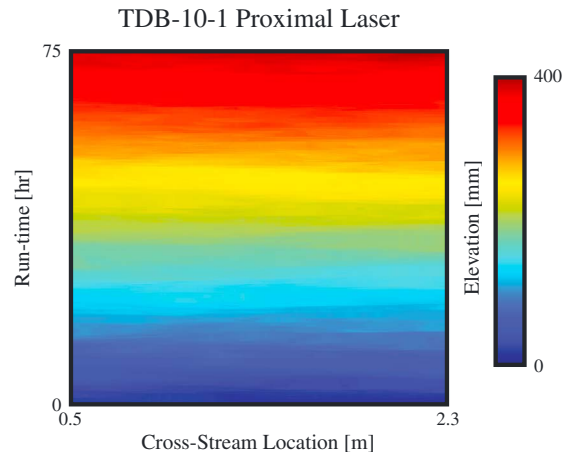


**Figure 4.** Space-time-elevation map defining evolution of topography and surface dynamics for the proximal measurement transect of the TDB-10-1 experiment. Map constructed from sequential delta-top profiles collected every 2 min of experiment.

**Table 2.** Internally Generated Experimental Parameters

		$\chi$	Wetted Fraction	$H_c$	$T_c$	$\kappa$
		(1/1)	(1/1)	(mm)	(h)	(1/1)
TDB-10-1	Proximal	0.43	0.36	18.5	3.70	0.66
	Medial	0.61	0.36	14.2	2.84	0.61
	Distal	0.78	0.38	11.1	2.23	0.56
TDB-10-2	Proximal	0.43	0.53	21.0	2.10	0.64
	Medial	0.61	0.54	18.9	1.89	0.60
	Distal	0.78	0.60	13.4	1.34	0.56
TDB-11-1	Proximal	0.41	0.49	21.0	4.20	0.70
	Medial	0.59	0.47	18.5	3.70	0.66
	Distal	0.76	0.54	13.7	2.74	0.62

[23] The final parameter of the delta morphologies that we characterize is the average down system slope. Using topographic measurements at the three transect locations, we measure the average down system slope along the center of the basin. TDB-10-1 and TDB-10-2 share similar slopes of 0.078 and 0.076, respectively. The average down system slope of TDB-11-1 was significantly less than the other two experiments at 0.061.

#### 4.1. Evolution of Accommodation Space

[24] Utilizing the topographic scans, we generate space-time maps of accommodation at the three measurement

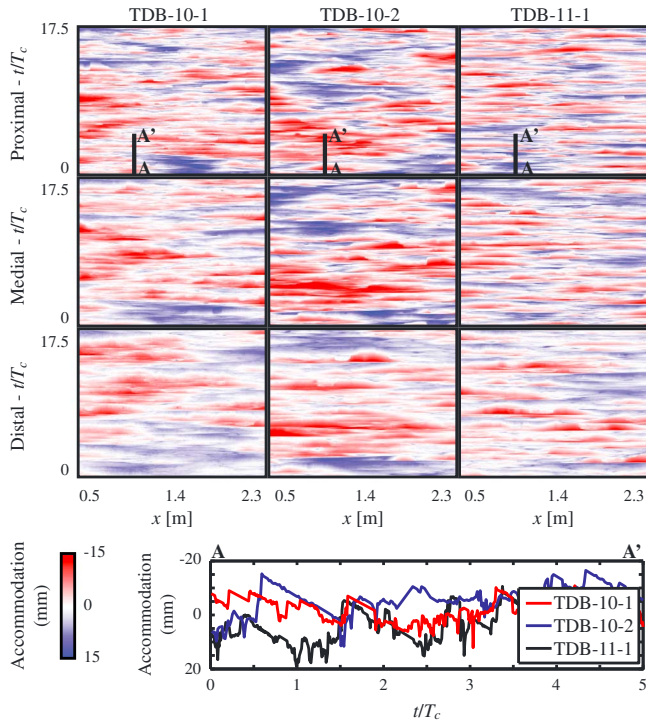


**Figure 5.** Accommodation maps in nondimensional time defining evolution of topography for the three measurement transect locations in the three experiments. Plot at base of figure displays example time series of accommodation measured at a single location on the proximal transect for the three experiments over an equivalent amount of nondimensional time.

transects for the three experiments. We define accommodation as the depth available for deposition below the theoretical long-term graded profile of a transport system [Mackin, 1948; Vail, 1987]. We start our analysis with the evolution of accommodation depth as this allows us to examine basin-filling trends in one dimension (1-D), in this case the vertical direction prior to moving to two dimensions. We estimate accommodation depth for all available space-time pairs in the three experiments by first detrending the space-time-elevation maps for the long-term deposition rate driven by imposed base-level rise. Next, we detrend each map for the long-term cross-stream topography at each measurement transect. This second step is necessary as the migration of channels over the delta top, originating at the basin infed location at the center of the proximal wall, resulted in an average symmetric convex up profile of topography for all strike-oriented transects, with on average the highest topography located in the center of the basin. In the resulting space-time-accommodation maps (Figure 5), positive values represent available accommodation depth (e.g., the topography at that space and time is below the graded profile for that location at that time) and negative values represent negative accommodation depth (e.g., the topography at that space and time is above the graded profile for that location at that time). The time-space maps of accommodation at the three measurement transects in the three experiments show that the basins filled via the accumulation of depositional and erosional events that are both discontinuous in time and space.

[25] We aim to compare time scales important to basin filling in our three experiments in both dimensional time and a nondimensional time constructed by dividing the time scale of interest,  $t$ , by  $T_c$ . The choice of nondimensionalizing  $t$  by  $T_c$  is done as Wang *et al.* [2011] proposed  $T_c$  to be the time scale at which basin-filling sedimentation trends switch from being partially influenced by autogenic processes to completely determined by allogenic forcings.  $T_c$  for each measurement transect for each experiment was calculated using imposed values of  $\bar{\tau}$  and measurements of  $H_c$ . Visual inspection of accommodation maps plotted as a function of space and nondimensional time suggests a similar spectrum of basin-filling time scales in TDB-10-1 and TDB-10-2 that have lower frequencies compared to events in TDB-11-1 (Figure 5).

[26] The space-time maps at each transect for each experiment show a range of accommodation ( $a$ ) values that span a negative to positive range. We use these maps to generate probability distribution functions, PDFs, of accommodation

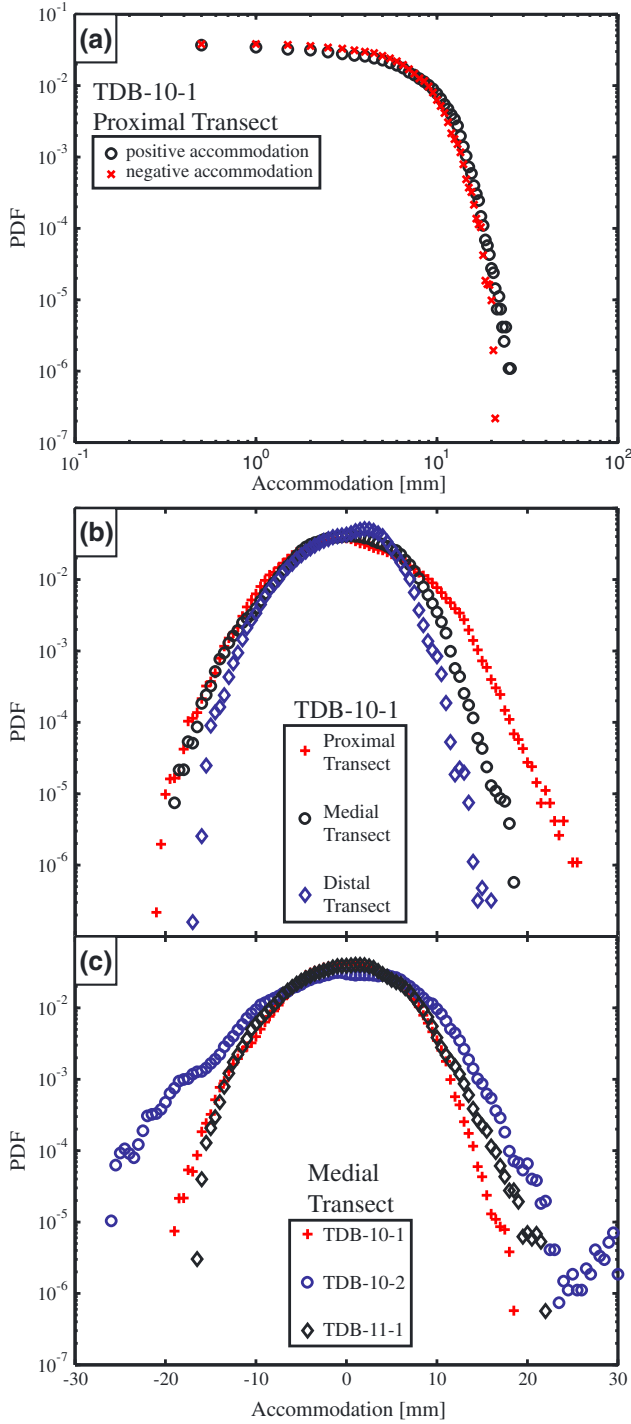


**Figure 6.** Probability density function of accommodation measurements. (a) Log-log plot of positive and negative accommodation measurements from the TDB-10-1 proximal measurement transect. (b) Comparison of accommodation distributions at the three measurement transects of TDB-10-1. (c) Comparison of accommodation distributions from the three experiments at the medial transect.

for each data set (Figure 6). We find the following results: (1) for each data set, the distribution of positive and negative accommodation values is roughly symmetric, (2) when plotted in log-log space, the distributions of positive and negative

accommodation appear to follow a truncated Pareto distribution, (3) the width of the distributions for each experiment narrows going from proximal to distal transects, and (4) at each transect location, TDB-10-2 has the widest distribution followed by TDB-11-1 and then TDB-10-1 (Figure 6). Finally, we note that the roll-off in probability of accommodation in log-log space for each data set, in example of which is given in (Figure 6a), occurs at a value similar to the  $H_c$  which characterizes each data set.

[27] To quantify the accommodation-filling time scales in the three experiments, we generate power spectra of accommodation for each transect in each experiment (Figure 7). All power spectra are computed on the ensemble of time series along each topographic transect. Power spectra of  $a(t)$  reveal the same general pattern for all transects. At short time scales, there is a nonstationary regime in which spectral density increases as a power-law function of period. This observation demonstrates that larger fluctuations in  $a$  have larger characteristic time scales and that correlation exists over a wide range of time scales. At longer time scales, however, we observe a rollover in spectral density after which it approaches an asymptotic upper limit. The general shape of these power spectra are similar to those generated in other numerical [Jerolmack and Paola, 2007] and physical experiments [Jerolmack and Paola, 2010] of sediment transport. In these earlier studies, the region of power-law growth in spectrum density is related to the range of autogenic processes operating in the transport system, while the rollover in spectral density is linked to truncated distributions of event sizes resulting from finite characteristics of a system [Jerolmack and Paola, 2010].

[28] Next we compare the spectral density of accommodation as a function of dimensionless time,  $a(t/T_c)$ , in our three

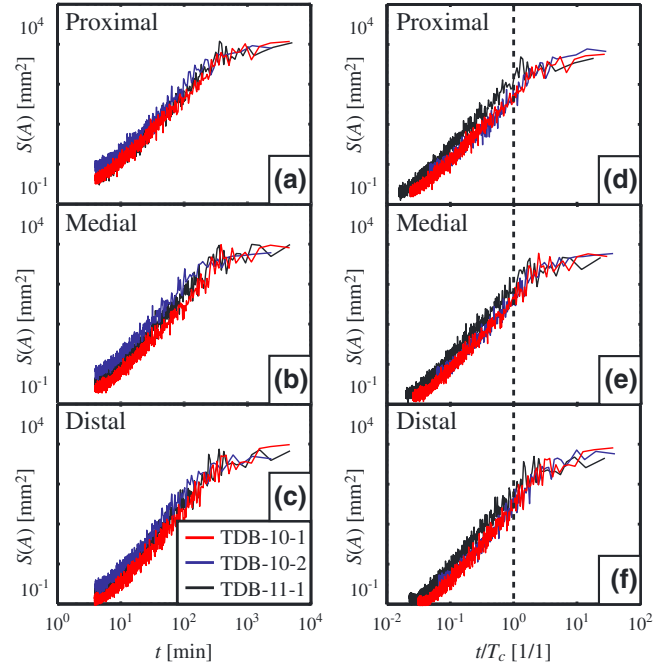


**Figure 7.** Ensemble-averaged power spectra of accommodation time series as a function of (a–c) dimensional and (d–e) dimensionless time in the three experiments at the three transect locations.

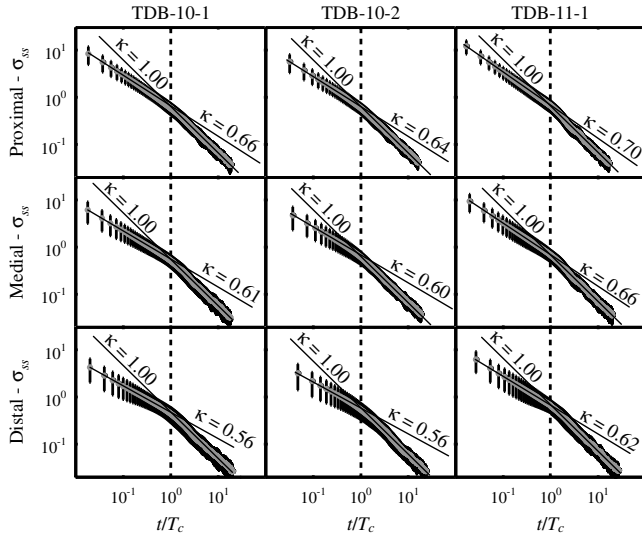


**Figure 8.** Comparison of the decay of  $\sigma_{ss}$  as a function of dimensionless time,  $t/T_c$ , for the three topography transects in the TDB-10-1, TDB-10-2, and TDB-11-1 experiments. Trend lines and associated  $\kappa$  values represent best-fit linear regression to log-log data with data in each plot separated into two segments at  $T_c$ . Error bars represent geometric standard deviation.

experiments (Figure 7). Following nondimensionalization of time, we make these observations. First, the rollover in the trend of spectral density as a function of  $t/T_c$ , which separates short time periods with power-law growth from long time periods, occurs at a time scale approximately equal to  $T_c$ . Second, at each measurement transect, the magnitude of spectral density is similar in TDB-10-1 and TDB-10-2 for all values of  $t/T_c$ . However, the magnitude of spectral density for TDB-11-1 is greater than the other two experiments for all  $t/T_c$  values less than 1. This indicates that in dimensionless time, space was filled in a statistically similar fashion in TDB-10-1 and TDB-10-2 which occurred at slightly lower frequencies than in the TDB-11-1 experiment.

#### 4.2. Strength and Time Scales of Compensation

[29] Next we turn to quantifying basin-filling trends in two dimensions (2-D) through use of the decay of  $\sigma_{ss}$  as a function of time. Utilizing the topographic data sets, we calculate  $\sigma_{ss}$  at each topographic transect for every possible pairwise combination of topographic surveys, allowing us to define the decay of  $\sigma_{ss}$  over time windows of 2–1000 min. Similar to Wang et al. [2011], we observe that the strength of compensation, as quantified by  $\kappa$ , is scale-dependent for all topographic transects in all experiments. We plot the decay of  $\sigma_{ss}$  as a function of  $t/T_c$  and find that for all data sets, the magnitude of  $\kappa$  over short time scales ( $t/T_c < 1$ ) is less than the magnitude of  $\kappa$  measured over long time scales ( $t/T_c > 1$ ) (Figure 8). For all data sets, the magnitude of  $\kappa$  below  $T_c$  is between 0.56 and 0.70, indicating that over these time scales, space is filled somewhere between randomly and compensationally. However, at time scales above  $T_c$ , all basins are filled purely compensationally, with  $\kappa$  equal to 1.

[30] Within individual experiments, the strength of compensation below  $T_c$  displays systematic changes in space, in

addition to systematic differences between experiments. First, we observe a decrease in  $\kappa$  from proximal to distal transects in each of the three experiments. In Figure 9A, we present measurements of  $\kappa$  for each experiment at each transect. We choose to display  $\kappa$  as a function of the dimensionless mass extraction parameter,  $\chi$ , which represents the fraction of supplied sediment flux lost to deposition up to a position  $x$  [Strong et al., 2005; Paola and Martin, 2012]. The flux lost to deposition is the integral of the net rate of deposition  $\bar{r}$  over

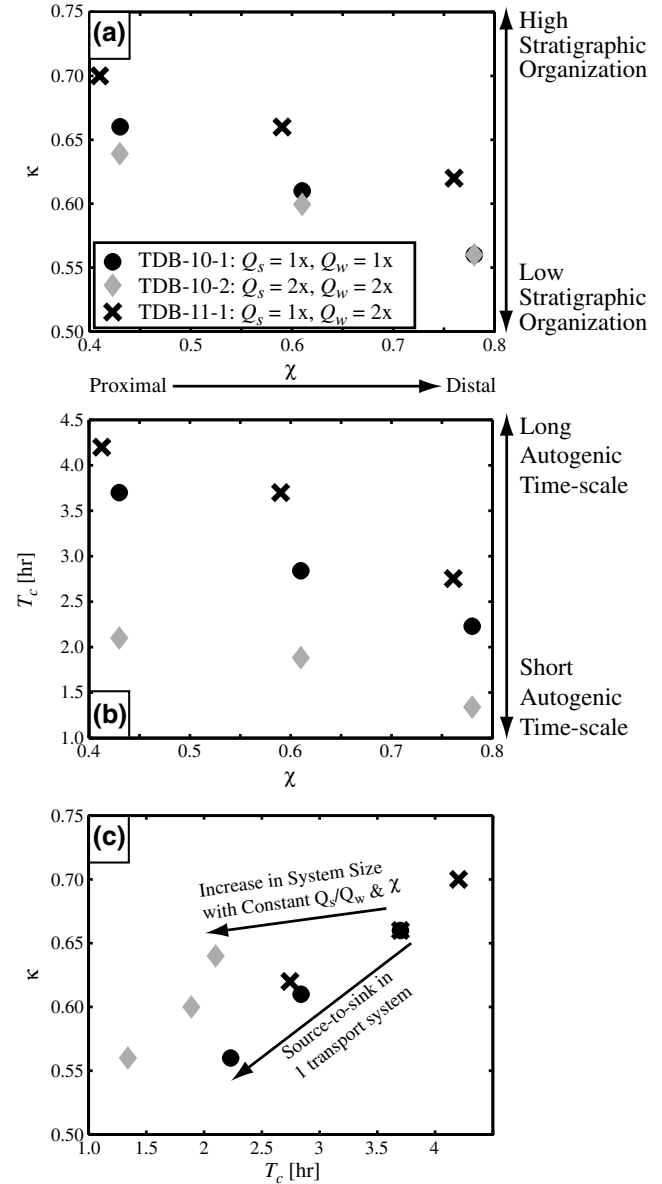


**Figure 9.** Data defining the strength and time scales of compensation observed in TDB-10-1, TDB-10-2, and TDB-11-1. (a) Comparison of the decay of  $\kappa$  with increasing  $\chi$  in the three experiments. Decreases in  $\kappa$  between 1.0 and 0.5 are associated with reductions in stratigraphic organization. (b) Comparison of the decay of  $T_c$  with increasing  $\chi$  in the three experiments. Decreases in  $T_c$  with  $\chi$  for any given experiment indicate a reduction in the time scales over which autogenic processes occur from source to sink. (c) Relationship of  $\kappa$  to  $T_c$  in each of the three experiments.

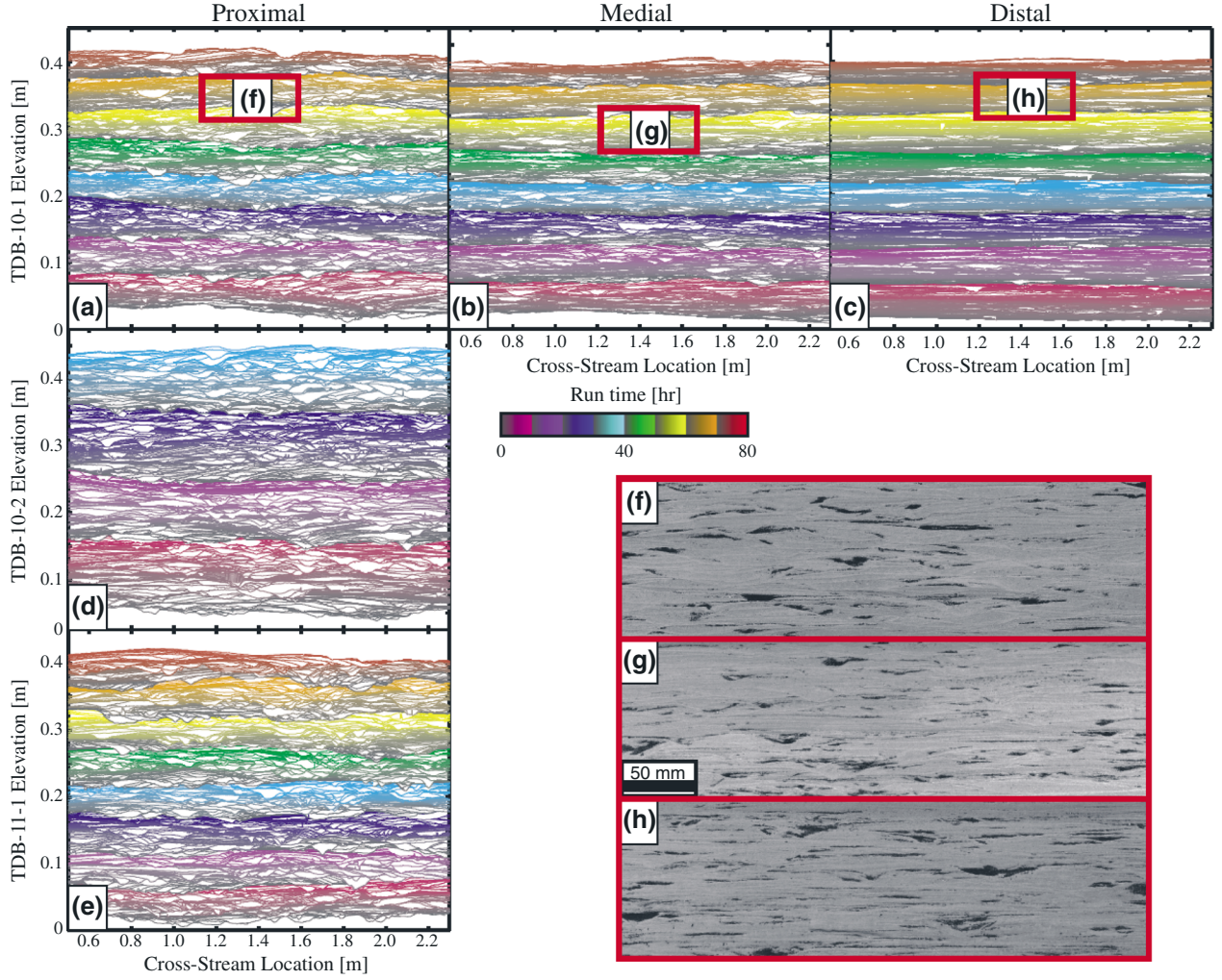


**Figure 10.** (a–c) Synthetic stratigraphic panels of final deposit architecture at the three measurement transects of TDB-10-1 and at the proximal measurement transect for the (Figure 10a, d, e) three experiments in addition to (f–h) images of the preserved physical stratigraphy at each transect from TDB-10-1. Red rectangles in the synthetic stratigraphic panels represent the location of the physical stratigraphy images.

the distance  $x$ . Thus, for an initial total sediment flux  $Q_{so}$ , the value of  $\chi$  at a given location is given by the total sediment flux lost to deposition normalized by  $Q_{so}$ , which for our basin geometry and boundary conditions can be determined as

$$\chi(x) = \frac{\bar{r}}{Q_{so}} \int_0^x B_w(x') dx' \quad (4)$$

where  $B_w$  represents the wetted width of the delta top at a given  $x$  distance. The use of  $\chi$  allows for the comparison of stratigraphic organization in our experiments to field-scale stratigraphy. The decay of  $\kappa$  with  $\chi$  indicates a decrease in stratigraphic organization from proximal to distal locations in our experiments.

[31] A comparison of the three experiments reveals that at all transect locations TDB-11-1 has a higher  $\kappa$  value than the other two experiments, TDB-10-1 and TDB-10-2, which share similar  $\kappa$  values at all transect locations. This indicates that the experiment with the highest ratio of  $Q_w:Q_s$  has the highest degree of stratigraphic organization, while the two

experiments associated with the same ratio of  $Q_w:Q_s$  shared similar stratigraphic organization.

[32] Within individual experiments,  $T_c$  also shows systematic changes in space, in addition to systematic changes between experiments. For each experiment, we observe a decrease in  $T_c$  as a function of  $\chi$ . This indicates that the maximum time scale over which autogenic processes occur decreases from source to sink in our experiments. At any value of  $\chi$ , TDB-11-1 has the longest  $T_c$ , followed by TDB-10-1 and then TDB-10-2 (Figure 9b).

### 4.3. Experimental Strata

[33] At the end of the aggradational stage of each experiment, the ocean level was slowly lowered and the delta basin drained. Following a drying phase, the experimental deposits were vertically sectioned at the three laser transects in order to observe the final deposit stratigraphy. As discussed above, the difference in density of the quartz ( $2650 \text{ kg/m}^3$ ) versus anthracite ( $1700 \text{ kg/m}^3$ ) results in differences in their relative mobility. The lighter anthracite particles tend to be more

mobile than the quartz grains and are therefore a proxy for fine sediment. This difference in mobility is recorded in the deposit where the anthracite and quartz often form distinct depositional bodies, such as channel fills and lobes. This texture aids our analysis of the experimental stratigraphy. Additionally, synthetic stratigraphy is generated from stacked delta-top profiles with topography clipped to account for sediment removed during erosion [Martin *et al.*, 2009].

[34] Utilizing the physical and synthetic stratigraphy (Figure 10) at the three measurement transects in the three experiments, we make the following observations. First, the strata at the three transects primarily consist of two facies: incisional channel-scour fill structures and tabular sheets. In contrast to the laterally constrained high-curvature channel bodies, the sheet-like deposits are laterally extensive low-curvature features. Next, we observe a decrease in the density of preserved channel-form bodies from proximal to distal transects in the basin, in addition to a decrease in the width and depth of preserved channels. A comparison of the three experiments reveals that the width and depth of channels in the two experiments with high  $Q_w$  (TDB-10-2 and TDB-11-1) were on average greater than those of the low  $Q_w$  experiment (TDB-10-1).

## 5. Discussion

### 5.1. Space Filling in 1-D

[35] Power spectra of accommodation time series all share a similar structure characterized by a power-law growth of spectral density over short time scales prior to saturating at long time scales. Space-time maps and PDFs of accommodation reveal several attributes of the basin-filling trends that might influence the structure of the power spectra. First, maps of accommodation clearly show a degree of structure indicating the presence of correlation in both space and time. Second, clear upper bounds exist for the positive and negative accommodation distributions in all data sets. Upper bounds on distributions of variables in real world systems are common and occur due to constraints set by physical mechanisms that govern the evolution of the system [Zhang *et al.*, 2007; Ganti *et al.*, 2011]. The upper limits for positive accommodation in our experiments are likely associated with the maximum depth of channels that can incise into the delta top, thus creating accommodation to be filled. The upper limits for negative accommodation are likely linked to the maximum amount of topography that can be constructed through sedimentation prior to complete diversion of flow.

[36] We analyze the influence of correlation and bounds on positive and negative accommodation for power spectrum through the generation of synthetic time series. We start by generating time series of accommodation through a random walk model with a lag-one autoregression, or Markov scheme

$$a_t = a_{t-1} + \varphi da_{t-1} + da \quad (5)$$

where  $\varphi$  is a constant that represents the degree of correlation of the accommodation increments in the system and  $da$  is chosen at random for each time step. For simplicity, in all models discussed,  $da$  is pulled from a normal distribution described by a zero mean and a standard deviation of 1. Further, all synthetic data sets consist of 2000 realizations, each with 2000 time steps, similar to the dimensions of our

space-time-accommodation maps. Example time series of accommodation generated with equation (5) are shown in Figure 11. In Figure 12a, we present resulting power spectra from synthetic accommodation time series generated with equation (5) and  $\varphi$  values equal to 0.00, 0.25, 0.50, 0.75, and 0.90. We find that in all models, the density of the power spectra grows as power-law functions of measurement time scale and that as the degree of correlation increases, the density of the power spectra at all time scales increases.

[37] Next, we implement a scheme to constrain time series of accommodation between predefined upper limits of positive and negative accommodation. We accomplish this by generating time series using equation (5), but define that if an accommodation increment ( $\varphi da_{t-1} + da$ ) results in an  $a_t$  value outside our limits of positive and negative accommodation, we generate new random accommodation increments until one is selected that will bring accommodation within our limits. Here, we stress that this scheme is not meant to represent the exact physics at operation in our experiments but is just meant to explore the influence on time series power spectra of accommodation bounds. For all models presented here, we keep the upper limit of positive accommodation equal to the upper limit of negative accommodation. We find that as the bounds placed on our synthetic accommodation time series are reduced, the region of power-law growth in spectral density is also reduced (Figure 12b). The resulting power spectra for time series with predefined bounds are then characterized by power-law growth in spectral density over short time scales prior to saturating at a given value for all longer time scales.

[38] Finally, we explore how nondimensionalizing time by  $T_c$  influences power spectra. Our experimental accommodation time series are generated from data sets with long-term elevation drift. As our synthetic accommodation time series are generated directly from equation (5), we lack  $\bar{r}$  to calculate  $T_c$ . For the sake of this analysis, we assume each of the synthetic accommodation time series are generated from elevation time series with  $\bar{r}$  equal to 1 unit per time step. As accommodation bounds in our experiments are well approximated by  $H_c$ , we calculate  $T_c$  here using the upper bound we place on our accommodation time series. Following this nondimensionalization, we find that power spectra, for all models run with accommodation bounds, saturate at roughly the same value of  $t/T_c$ , regardless of the exact bounds used, similar to what is observed in our experiments (Figure 12c). It is important to note that unlike our experimental data, this saturation does not occur at a value of  $t/T_c$  equal to 1 in the synthetic models. This is likely due to the fact that the magnitude of elevation increments in these synthetic models is determined by our choice of the shape of the elevation increment distribution, rather than being a function of the basin boundary conditions, as occurs in our experiments.

[39] The results from our experiments and synthetic time series suggest that even in basins with constant boundary conditions, autogenic processes result in fluctuations of surface topography that influence accommodation available for deposition over a wide range of time scales. In our experiments, we see a growth in the spectral density out to time scales equal to or slightly exceeding  $T_c$ . However, physical constraints on systems, for example, the maximum depth of channels or the maximum elevation of constructional topography possible prior to complete flow diversion, set upper limits on the time scales of autogenic processes in systems.

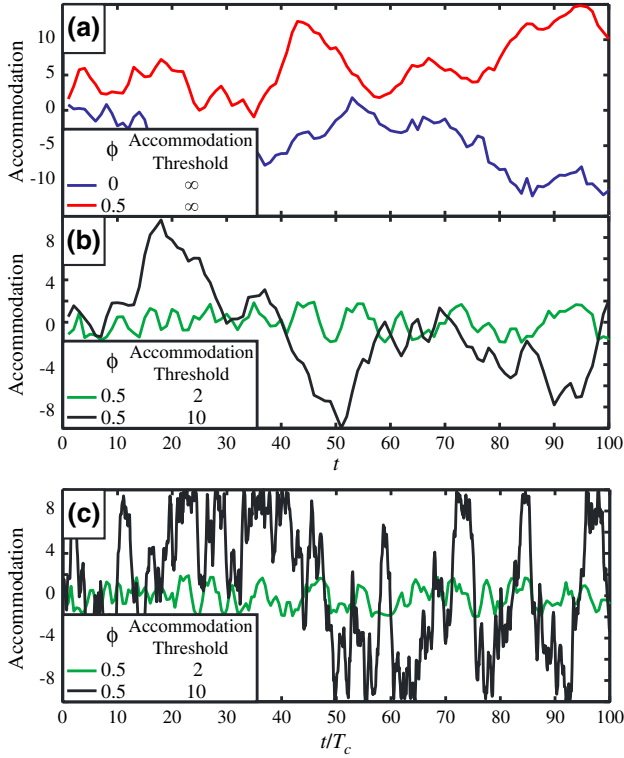


**Figure 11.** Synthetic time series of accommodation. (a) Time series resulting from models without upper and lower limits of accommodation but varying degrees of correlation. (b) Time series resulting from models with  $\phi$  equal to 0.5, but with two sets of upper bounds on positive and negative accommodation.

## 5.2. Influence of $Q_w$ and $Q_s$ on Long Time-Scale Autogenic Processes

[40] The central goal of our study is to characterize how changes in the absolute magnitude of  $Q_w$  and  $Q_s$  and changes in their relative ratio influence basin-filling sedimentation patterns. To address the influence of the absolute magnitude of  $Q_w$  and  $Q_s$ , we compare TDB-10-1 and TDB-10-2. Recall that  $Q_w$ ,  $Q_s$ , and  $\bar{\tau}$  of TDB-10-2 were double those of the control experiment, TDB-10-1. As a result, the size (depth and width) of the experimental channels increased in TDB-10-2 relative to TDB-10-1, while the size of the basin they filled remained fixed. Despite the twofold increase in these boundary conditions, when  $t$  is normalized by  $T_c$ , we observe near identical spectral density for time series of accommodation in the two experiments (Figure 7). Further, the strength of compensation, and thus stratigraphic organization, is near identical for the two experiments at each measurement transect. Taken together, these two results indicate that two systems, one small and one large, which share the same ratio of  $Q_w:Q_s$  fill space in a statistically similar fashion, but over different time scales. Regarding this last point, we note that at each measurement transect, the time scale of compensation was shorter for TDB-10-2 compared to TDB-10-1 and thus, the range of time scales at which autogenic processes operate was shorter in TDB-10-2 compared to TDB-10-1.

[41] While changes in the absolute magnitude of  $Q_w$  and  $Q_s$  did not influence the degree of organization in basin-filling sedimentation patterns, or the structure of accommodation

time series, the ratio of  $Q_w:Q_s$  does influence these parameters. To address the influence of the absolute magnitude of  $Q_w$  and  $Q_s$ , we compare TDB-10-1 and TDB-11-1. Recall that while  $Q_w$  of TDB-11-1 was doubled relative to the control experiment, all other parameters were held constant. The increase in  $Q_w$  resulted in deeper channels in TDB-11-1 relative to TDB-10-1. As a result, while the long-term average sedimentation rates were equal, TDB-11-1 had significantly longer  $T_c$  values at the three transects. Theoretical, experimental, and numerical studies have all observed a correlation between  $H_c$  and  $Q_w:Q_s$  [Parker *et al.*, 1998a; Parker *et al.*, 1998b; Powell *et al.*, 2012]. As such, our results suggest that the range of time scales over which autogenic processes operate in field systems is positively correlated with  $Q_w:Q_s$ . Next, time series of accommodation reveal that, following normalization of  $t$  by  $T_c$ , fluctuations in accommodation occur at higher frequencies in TDB-11-1 compared to the other two experiments (Figure 7). Finally, basin-filling sedimentation patterns are characterized by higher  $\kappa$  values in TDB-11-1 compared to the other two experiments. Taken together, our results clearly show that the ratio of  $Q_w:Q_s$  influences the organization of basin-filling sedimentation patterns more than the absolute magnitude of these parameters (Figure 9c). They also suggest that stratigraphic organization increases as a function of  $Q_w:Q_s$ . Thus, we would expect large deltaic systems, with relatively high values of  $Q_w:Q_s$ , to display more organization in their basin-filling sedimentation patterns compared to alluvial fans constructed at the outlet of bedrock canyons, characterized by low values of  $Q_w:Q_s$ . More work still needs to be done, though, to produce a predictive relationship between  $Q_w$  and  $Q_s$  for autogenic basin-filling sedimentation

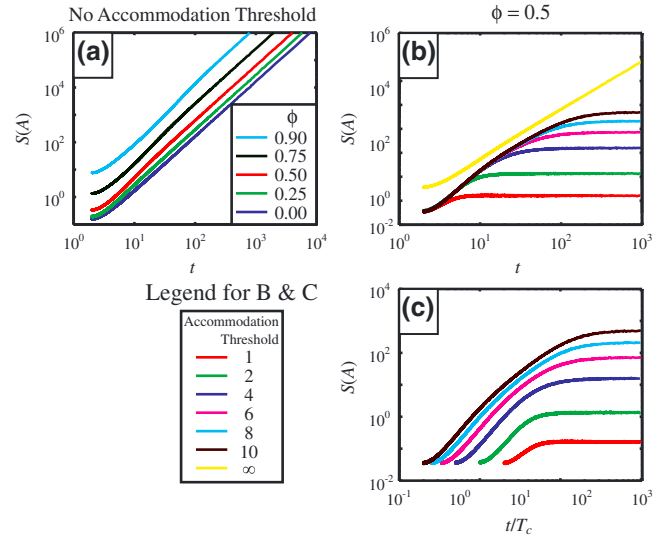


**Figure 12.** Average power spectra of synthetic accommodation time series. All time series constructed with accommodation increments pulled from normal distribution with zero mean and standard deviation of one. (a) Power spectra resulting from time series without upper and lower limits of accommodation but with varying degrees of correlation. Power spectra resulting from time series with  $\phi$  equal to 0.5, but with sequentially decreasing upper bounds on positive and negative accommodation plotted against (b) dimensional and (c) nondimensional periodicity.

**Table 3.** Compilation of Data Used to Define  $T_c$  for 13 Deltas

System #	Delta Name	Duration of Measurement (Myrs)	$H_c$ (m)	Sedimentation Rate (mm/year)	$T_c$ (kyr)	Reference
1	Rio Grande	0.12	4	0.71	5.6	[Banfield and Anderson, 2004]
2	Niger	1.8 ± 1.4	5	0.71 ± 0.4	7.0	[Chukwueke and Thomas, 1992]
3	Orinoco	0.4	40	2.7	14.8	[Wood, 2000]
4	Po	1.45	17	1.0	17.0	[Carminati and Martinelli, 2002]
5	Rhine	2.5	4	0.15 ± 0.05	26.7	[Zagwijn, 1989]
6	Baram	2.58	12	0.43	27.9	[Saller and Blake, 2003]
7	Nile	2.8 ± 1.3	11	0.39 ± 0.21	28.2	[Abu El-Ella, 1990]
8	Yellow	0.2	20	0.6	33.3	[Cui et al., 2008]
9	Mackenzie	1 ± 0.8	9	0.12 ± 0.06	72.6	[Wang and Evans, 1997]
10	Ganges	3.9 ± 1.2	30	0.31	96.8	[Worm et al., 1998; Lindsay and Holliday, 1991]
11	Mississippi	5	30	0.25	120.0	[Straub et al., 2009]
12	Indus	5	16	0.12	133.3	[Clift et al., 2002]
13	Yangtze	2.6	14	0.09 ± 0.05	155.6	[Chen and Stanley, 1995]

patterns as our experiments only cover a narrow window in these allogenic forcings.

### 5.3. Changes From Source To Sink

[42] In our experiments, we notice several changes in basin-filling patterns and stratigraphic architecture which occur in each of the three experiments. Similar to stratigraphic architecture of field-scale alluvial fans [Nichols and Fischer, 2006], in the proximal zone of our experiments, we observe highly amalgamated and interconnected stacked channel bodies with high quartz to anthracite ratios. Medial zones are characterized by a lower channel body density, but increased density of sheet sand bodies. Finally, the distal zones are characterized by sheet terminal splay deposits, small channels, and low quartz to anthracite ratios. These source to sink changes in stratigraphic architecture are associated with a decrease in organization of basin-filling patterns, as characterized by  $\kappa$ , in all experiments. At present, we do not fully understand the morphodynamics that result in the downstream decay of organization in basin-filling trends. However, this trend might be related to an observed decrease in the variance of deposition rate from source to sink or the observed reduction in-channel density.

[43] Finally, in all experiments, we note a decrease in  $T_c$  from sediment source to sink. This last trend is primarily a result of the decrease in  $H_c$  with transport distance in our experiments, as the long-term sedimentation rate was spatially constant in our experiments and set by the imposed base-level rise rate. For field-scale systems with near spatially uniform deposition rates, our results suggest that preservation of environmental signals is optimized at distal settings where the range of time scales over which autogenic processes operate is minimized. However, in systems with spatially variable subsidence and therefore spatially variable long-term sedimentation rates, this source to sink reduction in  $T_c$  might not hold. In these settings, we suggest that the preservation of environmental signals in stratigraphy would still be maximized where  $T_c$  is minimized. Thus, for basins with a cross-stream subsidence gradient characterized by near zero subsidence rates along basin margins and maximum subsidence rates near the basin center, we suggest that signals would be best preserved in the center of the basin.

### 5.4. Time Scale of Compensation in Field-Scale Systems

[44] Similar to the findings of Wang et al. [2011], we find that the strength of compensation is scale-dependent in our three experiments (Figure 8). For all cases,  $\kappa$  increases with stratigraphic scale until saturating at a value of 1.0. Further, the time scale at which these systems transition to pure compensation ( $\kappa=1.0$ ) is correctly predicted by equation (3). Equation (3) essentially states that the geometry of deposits carries the signature of stochastic autogenic dynamics out to a time scale equal to the time necessary to fill a basin to a depth equal to the amount of surface roughness in a transport system. Wang et al. [2011] estimated  $T_c$  for the Lower Mississippi Delta region using known depths of the Mississippi River and long-term sedimentation rates from biostratigraphic information. Here we compile a larger data set of  $T_c$  estimates for field-scale basins using published data on river depths and long-term sedimentation rates, and include 13 modern delta systems (Table 3 and Figure 13). When

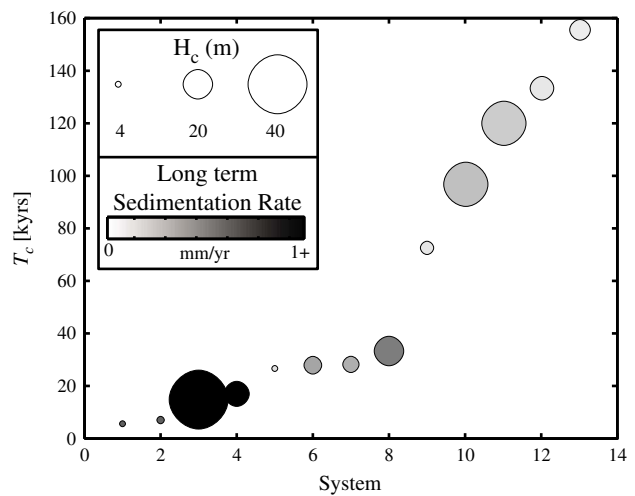


**Figure 13.**  $T_c$  estimates for compilation of 13 modern delta systems using published data on channel depth and long-term deposition rate (measurement interval in excess of 100 kyr). Size of circle scales with the depth of a system's channels while grayscale value of filled circles scales with the long-term sedimentation rate of a basin.

compiling our data set, we only utilized sedimentation rates that were measured for time intervals in excess of 100 kyrs. As shown by *Sadler* [1981] and *Strauss and Sadler* [1989], for a wide range of time scales, sedimentation rate is a function of the interval of measurement. However, *Jerolmack and Sadler* [2007] showed that persistence in deposition rates as a function of measurement interval is reached at time scales in excess of 100 kyr for deltas.

[45] For the 13 systems in our compilation, we estimate  $T_c$  values between 5.6 and 156 kyr. On average, systems with low  $T_c$  are in basins with low channel depths and high long-term sedimentation rates, while systems with high  $T_c$  values are in basins with deep channels and low long-term sedimentation rates (Figure 13). Importantly, the duration of  $T_c$  for many of these systems overlaps or is longer than the period of the Earth's eccentricity (100,000 year), inclination (70,000 year), obliquity (41,000 year), axial precession (26,000 year), or apsidal precession (21,000 year) cycles. These Milankovitch cycles impact the amount and distribution of solar radiation entering the atmosphere, specifically the amount of solar radiation entering the atmosphere during summer months at high latitudes [*Hinnov*, 2000]. These changes in solar radiation strongly influence the size of high latitude glaciers and thus directly impact global eustasy, a commonly discussed allogenic forcing.

[46] In addition to climate cycles and their influence on global eustasy, it is also important to note that the time scale of compensation for many sedimentary systems overlaps commonly discussed tectonic time scales. For example, it has been hypothesized that earthquakes cluster in time on some fault systems [*Prosser*, 1993; *Dorsey et al.*, 1997; *Gupta et al.*, 1998; *Gagliano*, 2005]. This clustering would result in long time periods with little or no movement along a fault section (and thus little generation of accommodation along normally faulted basins experiencing constant eustasy) followed by periods of rapid movement and an increase in accommodation. Much of the evidence supporting earthquake clusters come from the interpretation of cyclicity in stratigraphic patterns that are assumed to record allogenic forcings. For example *Dorsey et al.* [1997] used cyclicity in stratigraphic architecture of Pliocene Gilbert-type deltas in the Loreto basin, Baja California Sur, Mexico to argue for earthquake clustering with frequencies between 300 and 40,000 year. Additional studies in the Dead Sea graben and Xiaojiang fault zone of China suggest tectonic cycles with periods of 20,000–30,000 year [*Marco et al.*, 1996; *Xu and Deng*, 1996]. Coupled with climatic cycles, the subsidence cycles composed of relatively active and quiescent intervals would further complicate the interpretation of allogenic forcings in the sedimentary record. These examples highlight the overlapping time scales of climate and tectonic forcings, in addition to autogenic processes. They also point to the care that must be taken by stratigraphers in accurately distinguishing between the products of allogenic forcings and autogenic processes in the preserved record.

## 6. Summary

[47] Utilizing physical experiments, we examine the strength and time scales of autogenic processes in alluvial basins and how these processes are influenced by the absolute magnitudes of  $Q_w$  and  $Q_s$ , and their relative ratio.

Building on prior studies, we use techniques to quantify autogenic processes in one and two (cross-stream direction) dimensions as well as changes along a source to sink path. The main results are summarized as follows:

[48] 1. Utilizing time series of detrended elevation (basin accommodation) and measurements of compensation strength, we characterize autogenic processes in our experiments. We find that the ratio of  $Q_w:Q_s$  influences the magnitudes of autogenic processes and the resulting degree of organization in basin fill more than the absolute magnitude of these parameters. As a result, systems with similar ratios of  $Q_w:Q_s$ , but with different magnitudes of  $Q_w$  and  $Q_s$ , fill basins in a statistically similar fashion, just over different time and space scales. We find that the degree of organization in basin-fill patterns, as characterized by  $\kappa$ , increases with the ratio of  $Q_w:Q_s$ . This finding suggests that stratigraphy constructed by large deltas, typically characterized by high  $Q_w:Q_s$ , will display more organization in basin-fill patterns compared to alluvial fans constructed at the terminus of bedrock canyons, which are typically characterized by low  $Q_w:Q_s$ .

[49] 2. We observe a decay in stratigraphic organization, quantified through the compensation index, from sediment source to sink in each of our experiments. This decay in stratigraphic organization is correlated to a reduction in channel body density in the resulting stratigraphy. These observations suggest that a predictable relationship between stratigraphic organization and nondimensional distance along a sediment transport systems might exist, following normalization for  $Q_w:Q_s$ , and could aid in the modeling and prediction of field-scale stratigraphic architecture.

[50] 3. Similar to previously published work [*Wang et al.*, 2011], we find compensation to be scale-dependent. In our experiments, basin-fill patterns do not completely match pseudo subsidence patterns until a time-scale set by the depth of a system's channels divided by the long-term basin-wide deposition rate. We compile a data set of 13 modern delta systems where channel depth and long-term deposition rate are known. Estimated compensation time scales in these basins range between 5 and 150 kyr. These time scales overlap many long time scale climatic and tectonic signals, and thus likely complicate our ability to extract the record of allogenic signals from stratigraphy. On a positive note, quantitatively constraining the strength and time scales of autogenic processes will aid our recognition of signals stored in stratigraphy which are definitively related to allogenic forcings.

[51] **Acknowledgments.** We thank J. Kuykendall, whose expertise made the experiment described in this work possible; C. Esposito, Q. Li, K. Pennuto, and A. Breaux helped conduct the experiments discussed in the text; B. Sheets and C. Paola for developing the idea to monitor the decay of the standard deviation of sedimentation/subsidence that gave birth to this study; Peter Sadler for sharing data on delta sedimentation rates; and E. Hajek for stimulating discussions that motivated and clarified several ideas in this manuscript. The editorial staff of *JGR-Earth Surface*, Peter Sadler, and an anonymous reviewer are thanked for constructive reviews. We gratefully acknowledge support by National Science Foundation grant EAR-1024443 to Straub.

## References

- Abu El-Ella, R. (1990), The Neogene-quadernary section in the Nile Delta, Egypt: Geology and hydrocarbon potential, *J. Pet. Geol.*, 13(3), 329–340.
- Allen, J. R. L. (1978), Studies in fluvial sedimentation: An exploratory quantitative model for the architecture of avulsion-controlled alluvial sites, *Sediment. Geol.*, 26, 617–644.

- Banfield, L. A., and J. B. Anderson (2004), Late Quaternary Evolution of the Rio Grande Delta: Complex Response to Eustasy and Climate Change, in *Late Quaternary Stratigraphic Evolution of the Northern Gulf of Mexico Margin*, SEPM Special Publication No. 79, edited by J. B. Anderson and R. H. Fillon, pp. 289–306, SEPM (Society for Sedimentary Geology), Tulsa, OK.
- Bryant, M., P. Falk, and C. Paola (1995), Experimental study of avulsion frequency and rate of deposition, *Geology*, 23(4), 365–368.
- Carminati, E., and G. Martinelli (2002), Subsidence rates in the Po Plain, northern Italy: The relative impact of natural and anthropogenic causation, *Eng. Geol.*, 66, 241–255.
- Chen, Z., and D. J. Stanley, (1995), Quaternary Subsidence and River Channel Migration in the Yangtze Delta Plain, Eastern China, *Journal of Coastal Research*, 11(3), 927–945.
- Chukwueke, C., G. Thomas, and J. Delfaud (1992), Processus sédimentaires, eustatisme, subsidence et flux thermique dans la partie distale du Delta du Niger, *Bulletin des Centre de Recherches Exploration-Production Elf-Aquitaine*, 16(1), 137–186.
- Clarke, L., T. A. Quine, and A. Nicholas (2010), An experimental investigation of autogenic behaviour during alluvial fan evolution, *Geomorphology*, 115(3–4), 278–285, doi:10.1016/j.geomorph.2009.06.033.
- Clift, P., C. Gaedicke, R. Edwards, J. I. Lee, P. Hildebrand, S. Amjad, R. S. White, and H. U. Schuler (2002), The stratigraphic evolution of the Indus Fan and the history of sedimentation in the Arabian Sea, *Mar. Geophys. Res.*, 23(3), 223–245.
- Cui, S., H. Liu, S. Tong, J. Zhang, Z. Wu, and J. Wu, (2008), Seismic stratigraphy of the quaternary Yellow River delta, Bohai Sea, eastern China, *Mar. Geophys. Res.*, 29, 27–42.
- Deptuck, M. E., D. J. W. Piper, B. Savoye, and A. Gervais (2008), Dimensions and architecture of late Pleistocene submarine lobes off the northern margin of East Corsica, *Sedimentology*, 55(4), 869–898.
- Dorsey, R. J., P. J. Umhoefer, and P. D. Falk (1997), Earthquake clustering inferred from Pliocene Gilbert-type fan deltas in the Loreto basin, Baja California Sur, Mexico, *Geology*, 25(8), 679–682.
- Edmonds, D. A., and R. L. Slingerland (2010), Significant effect of sediment cohesion on delta morphology, *Nat. Geosci.*, 3(2), 105–109, doi:10.1038/Ngeo730.
- Gagliano, M. S. (2005), Effects of earthquakes, fault movements, and subsidence on the south Louisiana landscape, *The Louisiana Civ. Eng. J.*, 13(2), 19–22.
- Ganti, V., K. M. Straub, E. Fofoula-Georgiou, and C. Paola (2011), Space-time dynamics of depositional systems: Experimental evidence and theoretical modeling of heavy-tailed statistics, *J. Geophys. Res.-Earth*, 116, F02011, doi:10.1029/2010JF001893.
- Gupta, S., P. A. Cowie, N. H. Dawers, and J. R. Underhill (1998), A mechanism to explain rift-basin subsidence and stratigraphic patterns through fault-array evolution, *Geology*, 26(7), 595–598, doi:10.1130/0091-7613.
- Hajek, E. A., P. L. Heller, and B. A. Sheets (2010), Significance of channel-belt clustering in alluvial basins, *Geology*, 38(6), 535–538.
- Hajek, E. A., P. L. Heller, and E. L. Schur (2012), Field test of autogenic control on alluvial stratigraphy (Ferris Formation, Upper Cretaceous–Paleogene, Wyoming), *Geol. Soc. Am. Bull.*, 124(11–12), 1898–1912, doi:10.1130/B30526.1.
- Heller, P. L., C. Paola, I. Hwang, B. John, and R. Steel (2001), Geomorphology and sequence stratigraphy due to slow and rapid base-level changes in an experimental subsiding basin (XES 96–1), *AAPG Bull.*, 85(5), 817–838.
- Hinnov, L. A. (2000), New perspectives on orbitally forced stratigraphy, *Annu Rev Earth Pl Sc*, 28, 419–475.
- Hofmann, M. H., A. Wroblewski, and R. Boyd (2011), Mechanisms controlling the clustering of fluvial channels and the compensational stacking of cluster belts, *J. Sediment. Res.*, 81(9–10), 670–685, doi:10.2110/Jsr.2011.54.
- Hoyal, D. C. J. D., and B. A. Sheets (2009), Morphodynamic evolution of experimental cohesive deltas, *J. Geophys. Res.-Earth*, 114, F02009, doi:10.1029/2007JF000882.
- Jerolmack, D. J., and C. Paola (2007), Complexity in a cellular model of river avulsion, *Geomorphology*, 91, 259–270.
- Jerolmack, D. J., and C. Paola (2010), Shredding of environmental signals by sediment transport, *Geophys. Res. Lett.*, 37, L19401, doi:10.1029/2010GL044638.
- Jerolmack, D. J., and P. Sadler (2007), Transience and persistence in the depositional record of continental margins, *J. Geophys. Res.-Earth*, 112, F03S13, doi:10.1029/2006JF000555.
- Karssenber, D., and J. S. Bridge (2008), A three-dimensional numerical model of sediment transport, erosion and deposition within a network of channel belts, floodplain and hill slope: Extrinsic and intrinsic controls on floodplain dynamics and alluvial architecture, *Sedimentology*, 55(6), 1717–1745.
- Kendall, C. G. S. C., J. Strobel, R. Cannon, J. Bezdek, and G. Biswas (1991), The simulation of the sedimentary fill of basins, *J. Geophys Res-Solid*, 96(B4), 6911–6929, doi:10.1029/90j01406.
- Kim, W., and C. Paola (2007), Long-period cyclic sedimentation with constant tectonic forcing in an experimental relay ramp, *Geology*, 35(4), 331–334.
- Kim, W., C. Paola, J. B. Swenson, and V. R. Voller (2006), Shoreline response to autogenic processes of sediment storage and release in the fluvial system, *J. Geophys Res-Earth*, 111(F4), F04013, doi:10.1029/2006JF000470.
- Kim, W., B. Sheets, and C. Paola (2010), Steering of experimental channels by lateral basin tilting, *Basin Res.*, 22(3), 286–301.
- Lindsay, J., D. W. Holliday, and A. G. Hulbert (1991), Sequence Stratigraphy and the Evolution of the Ganges-Brahmaputra Delta Complex, *AAPG Bull.*, 75, 1233–1254.
- Lyons, W. J. (2004), Quantifying channelized submarine depositional systems from bed to basin scale, PhD thesis, 252 pp., Massachusetts Institute of Technology, Cambridge.
- Mackey, S. D., and J. S. Bridge (1995), 3-Dimensional model of alluvial stratigraphy: Theory and application, *J. Sediment Res B*, 65(1), 7–31.
- Mackin, J. H. (1948), Concept of the graded river, *Geol. Soc. Am. Bull.*, 59, 463–512.
- Marco, S., M. Stein, A. Agnon, and H. Ron (1996), Long-term earthquake clustering: A 50,000-year paleoseismic record in the Dead Sea Graben, *J. Geophys Res-Sol Earth*, 101(B3), 6179–6191, doi:10.1029/95JB01587.
- Martin, J., C. Paola, V. Abreu, J. Neal, and B. Sheets (2009), Sequence stratigraphy of experimental strata under known conditions of differential subsidence and variable base level, *AAPG Bull.*, 93(4), 503–533.
- Mohrig, D., P. L. Heller, C. Paola, and W. J. Lyons (2000), Interpreting avulsion process from ancient alluvial sequences: Guadalupe-Matarranya (northern Spain) and Wasatch Formation (western Colorado), *GSA Bull.*, 112, 1787–1803.
- Mutti, E., and M. Sonnino (1981), *Compensational Cycles: A Diagnostic Feature of Turbidite Sandstone Lobes*, Paper Presented at Second European Regional Meeting, International Association of Sedimentologist, Bologna, Italy.
- Nichols, G. J., and J. A. Fischer (2006), Processes, facies, and architecture of fluvial distributary system deposits, *Sediment. Geol.*, 195, 75–90.
- Olariu, C., and J. P. Bhattacharya (2006), Terminal distributary channels and delta front architecture of river-dominated delta systems, *J. Sediment. Res.*, 76(1–2), 212–233.
- Paola, C., and J. M. Martin (2012), Mass-balance effects in depositional systems, *J. Sediment. Res.*, 82(5–6), 435–450, doi:10.2110/Jsr.2012.38.
- Paola, C., K. M. Straub, D. Mohrig, and L. Reinhardt (2009), The “unreasonable effectiveness” of stratigraphic and geomorphic experiments, *Earth - Sci. Rev.*, 97, 1–43.
- Parker, G., C. Paola, K. X. Whipple, and D. Mohrig (1998a), Alluvial fans formed by channelized fluvial and sheet flow I: Theory, *J. Hydraul. Eng.*, 124(10), 985–995.
- Parker, G., C. Paola, K. X. Whipple, D. Mohrig, C. M. Toro-Escobar, M. Halverson, and T. W. Skoglund (1998b), Alluvial fans formed by channelized fluvial and sheet flow. II: Application, *J. Hydraul. Eng.*, 124(10), 996–1004.
- Pitman, W. C. (1978), Relationship between eustacy and stratigraphic sequences of passive margins, *Geol. Soc. Am. Bull.*, 89(9), 1389–1403.
- Powell, E. J., W. Kim, and T. Muto (2012), Varying discharge controls on timescales of autogenic storage and release processes in fluvio-deltaic environments: Tank experiments, *J. Geophys Res-Earth*, 117, F02011, doi:10.1029/2011JF002097.
- Prosser, S. (1993), Rift-related linked depositional systems and their seismic expression, *Geological Society, London, Special Publications*, 71(1), 35–66.
- Saller, A., and G. Blake (2003), Sequence stratigraphy and syndepositional tectonics of upper Miocene and Pliocene deltaic sediments, offshore Brunei Darussalam, in *Tropical deltas of Southeast Asia - ISedimentology, stratigraphy, and petroleum geology: SEPM (Society for Sedimentary Geology) Special Publication 76*, edited by F. Hasan Sidi, pp. 219–234.
- Sadler, P. M. (1981), Sediment accumulation rates and the completeness of stratigraphic sections, *J. Geol.*, 89, 569–584.
- Sadler, P. M. (1993), Models of time-averaging as a maturation process: How soon do sedimentary sections escape reworking?, in *Taphonomic Approaches to Time Resolution in Fossil Assemblages*, *Paleontological Society, Short Courses in Paleontology*, v. 6, edited by S. M. Kidwell, and A. K. Behrensmeier, pp. 188–209, University of Tennessee, Knoxville, TN.
- Sheets, B. A., T. A. Hickson, and C. Paola (2002), Assembling the stratigraphic record: Depositional patterns and time-scales in an experimental alluvial basin, *Basin Res.*, 14, 287–301.
- Sheets, B. A., C. Paola, and J. M. Kelberer (2007), Creation and preservation of channel-form sand bodies in an experimental alluvial system, in *Sedimentary*

- Processes, Environments and Basins*, edited by G. Nichols et al., pp. 555–567, Blackwell Publishing, Oxford, U.K.
- Stow, D. A. V., and M. Johansson (2000), Deep-water massive sands: Nature, origin and hydrocarbon implications, *Mar. Pet. Geol.*, 17(2), 145–174.
- Straub, K. M., and C. R. Esposito (2013), Influence of water and sediment supply on the stratigraphic record of alluvial fans and deltas: Process controls on stratigraphic completeness, *J. Geophys. Res. Earth Surface*, 118, 13, doi:10.1002/jgrf.20061.
- Straub, K. M., C. Paola, D. Mohrig, M. A. Wolinsky, and T. George (2009), Compensational stacking of channelized sedimentary deposits, *J. Sediment. Res.*, 79(9), 673–688.
- Strauss, D., and P. M. Sadler (1989), Stochastic-models for the completeness of stratigraphic sections, *Math. Geol.*, 21(1), 37–59.
- Strong, N., B. A. Sheets, T. A. Hickson, and C. Paola (2005), A mass-balance framework for quantifying downstream changes in fluvial architecture, in *Fluvial Sedimentology VII, International Association of Sedimentologist, Special Publication 35*, edited by M. Blum, S. Marriott, and S. Leclair, pp. 243–253, Wiley-Blackwell, Oxford, U.K.
- Syvitski, J. P. M., et al. (2009), Sinking deltas due to human activities, *Nat. Geosci.*, 2(10), 681–686, doi:10.1038/Ngeo629.
- Vail, P. R. (1987), Seismic stratigraphy interpretation utilizing sequence stratigraphy: Part 1: Seismic stratigraphy interpretation procedure, in *Atlas of Seismic Stratigraphy (Vol. 27)*, AAPG Studies in Geology, edited by W. W. Bally, pp. 1–10, American Association of Petroleum Geologists, Tulsa, OK.
- Van Dijk, M., G. Postma, and M. G. Kleinans (2009), Autocyclic behaviour of fan deltas: An analogue experimental study, *Sedimentology*, 56(5), 1569–1589.
- Wang, Y., and M. E. Evans, (1997), Paleomagnetism of Canadian Arctic permafrost; Quaternary magnetostratigraphy of the Mackenzi Delta, *Can. J. Earth Sci.*, 34, 135–139.
- Wang, Y., K. M. Straub, and E. A. Hajek (2011), Scale-dependent compensational stacking: An estimate of autogenic time scales in channelized sedimentary deposits, *Geology*, 39(9), 811–814.
- Whipple, K. X., G. Parker, C. Paola, and D. Mohrig (1998), Channel dynamics, sediment transport, and the slope of alluvial fans: Experimental study, *J. Geol.*, 106(6), 677–693.
- Wood, L. J. (2000), Chronostratigraphy and tectonostratigraphy of the Columbus Basin, eastern offshore Trinidad, *AAPG Bull.*, 84(12), 1905–1928.
- Worm, H. U., A. M. M. Ahmed, N. U. Ahmed, H. O. Islam, M. M. Huq, U. Hambach, and J. Lietz (1998), Large sedimentation rate in the Bengal Delta: magnetostratigraphic dating of Cenozoic sediments from northeastern Bangladesh, *Geology*, 26, 487–490.
- Xu, X. W., and Q. D. Deng (1996), Nonlinear characteristics of paleoseismicity in China, *J. Geophys. Res. Sol Earth*, 101(B3), 6209–6231.
- Zagwijn, W. H. (1989), The Netherlands during the Tertiary and Quaternary. A case history of Coastal lowland evolution, *Geol. Mijnbouw*, 68, 107–120.
- Zhang, Y., D. A. Benson, and B. Baeumer (2007), Predicting the tails of breakthrough curves in regional-scale alluvial systems, *Ground Water*, 45(4), 473–484.